

Wildland Fire Detection from Space: Theory and Application

Donald R. Cahoon, Jr.¹, Brian J. Stocks², Martin E. Alexander³, Bryan A. Baum⁴, Johann G. Goldammer⁵

¹NASA-Langley Research Center,
21 Langley Boulevard,
Hampton, VA 23185 USA
d.r.cahoon@larc.nasa.gov

²Canadian Forest Service, Sault Ste. Marie, Ontario, Canada

³Canadian Forest Service, Edmonton, Alberta, Canada

⁴Langley Research Center, Hampton, VA USA

⁵Fire Ecology Research Group, University of Freiburg, Germany

Published in:

Biomass Burning and its Inter-Relationships with the Climate System,
Advances in Global Change Research series,
Innes, J.L., Verstraete, M.M., and Beniston, M. (Eds.),
Series Editor: M. Beniston,
Kluwer Academic Publishers, Dordrecht and Boston,
Pages 151-169, 2000.

Last Modified: February 15, 2000 4:05 pm

Abstract

New satellite instruments are currently being designed specifically for fire detection, even though to date the detection of active fires from space has never been an integral part of the design of any in-orbit space mission. Rather, the space-based detection of fires during the last two decades has been exploiting measurements obtained for other objectives. The current fire products have proved to be of great benefit and interest, but their usefulness is not fully understood. Part of the confusion about the utility of these measurements stems from the lack of detailed knowledge about the data and its acquisition. The remote sensing research community has spent considerable time and effort trying to rationalize the usefulness of existing satellite imagery for active fire detection. Unfortunately, uncertainties about instrument capabilities pervades much of this research and the true limits of fire detection from space have not been fully evaluated and understood.

To analyze the active fire detection capability of any instrument, the flow of energy from the source to the instrument and the instrument's response to that energy must be considered. For this reason, an approach has been developed that models the energy emitted from surface fires, allowing for the fact that fire is itself a variable phenomenon. The energy transmission is then modeled along its path through the atmosphere and through the instrument's optical system. A fundamental concern is in the estimation of the total surface area that emits the energy which defines a single pixel in the image. Unfortunately, most of the fire detection modeling done to date is based on a misconception about the pixel and its actual size. Rather than using the radiometric footprint size, the instantaneous-field-of-view (IFOV) is used to describe the 'resolution' of the instrument. In fact, the radiometric footprint is considerably larger than the IFOV and greatly affects the energy modeling used to estimate the fire detection thresholds of a particular instrument. Based on knowledge of the radiometric footprint, the fire detection capability of AVHRR, DMSP-OLS, and MODIS are reviewed.

“the pixel, the elementary unit of analysis in remote sensing..., is a delusion which may become a snare for the unwary”, P. Fisher (1997).

I. Introduction

Even though this original quotation by Fisher is aimed more at the concern of the use of image pixels in geographical information system (GIS) analyses, it captures the essence of a fundamental problem in most remote sensing studies. That is, the large majority of remote sensing investigators lack a basic understanding of what defines an image pixel on the ground. Typically, image pixels are treated as non-overlapping tiles in a two-dimensional array of values which, when displayed, renders itself into a digital scene. In the image's simplest sense, this is the case. However, this simple interpretation of an image avoids the realities of what the pixel really represents and how the image is constructed. And, unbeknownst to many, the results of our analyses are tainted with these artifacts of reality which lead to misinterpretations of our data and, even worse, show up as errors in our analyses. Often the limitations of our image data pass unnoticed, but even when they do not, there is no explanation available to explain or justify the seemingly mysterious results.

There is far more to understand about the pixel. In the strictest sense, the word pixel is short for 'picture element' and describes one data point in an image. Alternatively, the word footprint is used to describe the surface area on the ground whose integrated energy defines the value of the pixel. The people that use remote sensing data in the Earth sciences are from a wide variety of academic backgrounds; largely the sciences, but not always. The people that most likely understand what an image pixel represents are the instrument engineers. These two groups, remote sensing scientists and instrument engineers, do not interact frequently enough. Hence,

some of the essential information about a pixel is lost or neglected. The users of the image data do not always possess the academic tools to sift through the engineering data, analyses and publications that cloak the meaning of an image pixel. To make things worse, the engineers analyze data relative to its frequency components (wave domain), and scientists relative to its spatial variations (physical domain). In essence, the remote sensing community suffers from a mathematical communication problem between themselves and the instrument engineers. This paper will try to bridge the gap and convey a simple concept of an instrument, how the instrument defines the pixel, and what is the value in understanding the pixel through the application to fire detection modeling.

The satellite remote sensing of fire began in the late 1970s (Croft, 1978; Matson et al., 1987). Since this time the global importance of fire has become internationally recognized. Fire has also escalated to the forefront in the global carbon budget discussions (e.g. Kurz et al., 1995; Kasischke et al., 1995; Stocks et al., 1998). Even with this increased awareness and the global importance of fire, there has not been a satellite instrument specifically designed for fire detection that has been launched at the time of this writing. Two decades have passed since the launch of the first Advanced Very High Resolution Radiometer (AVHRR). Although there are numerous studies in the literature on fire detection, there is not a rigorous comparison in the literature that documents what the thresholds of fire detection are for the various existing instruments. For the AVHRR (Kidwell, 1991), the Defense Meteorological Satellite Program Operational Linescan System (DMSP-OLS) (Elvidge et al, 1996), and the Moderate Resolution Imaging Spectrometer (MODIS) (King et al., 1992) instruments, this paper will apply the knowledge of the actual image pixel size on the ground (radiometric footprint), the knowledge of fire behavior, the knowledge of

the energy transmission through the atmosphere and instrument optics, and model the fire detection limitations for these three polar-orbiting instruments. At each step along the way, actual imagery will be used to assess the performance of the model and its components.

II. Instruments and the Pixel

The simplest notion of a satellite imager can be seen in figure 1. An imaging instrument can be subdivided into three systems, the optics, the detector, and the electronics. The energy from the actual scene passes through the optics and impinges on the detector. The detector must respond to the energy that it receives and convert that energy into a signal. This signal is typically filtered and converted from analog to digital. However, some of the newer detector technology can acquire a digital signal directly. The final product of the instrument is to pass a digital value out which corresponds to a single observation: the pixel. It is easy to conceive how the definition of a pixel is completely reliant upon the system which acquires it. At each step through the instrument, the original input signal is modified slightly. This modification, or degradation, of the input signal occurs for a variety of reasons. Optical systems are not perfect and energy passing through the optics will not be perfectly focused on the detector due to effects like diffraction. Detectors have response delays that are a function of the detector material, the sampling time, and the rate of change in the input signal. As the signal passes through the electronic system, it is converted from analog-to-digital, filtered, and sampled. Each step further induces change to the input signal. In a mathematical sense, we are convolving the input signal with a numerical filter corresponding to each phase of the measurement process. The cumulative effect of these filters at each step through the instrument can be represented as a single mathematical filter for the entire system which defines how much the input signal has been modified. Thus, the resulting output

digital signal, our image pixel value, has been numerically modified by each component of the instrument and can never fully resolve the original scene.

The performance of an instrument, its ability to reproduce the original scene, is measured by engineers and reported as the modulation transfer function (MTF) (Smith, 1966). The units of the MTF are those of spatial frequency (e.g., cycles per kilometer) and the MTF is usually reported in the engineering documentation for each individual imaging instrument. To more thoroughly understand the MTF, examine figure 2. Figure 2a shows a pattern of black and white bars, which represents an input scene, that the instrument scans across. If the instrument were to reproduce the scene correctly, then each scan would result in a square wave whose amplitude would resolve all of the contrast between the black and white bars, or in other terms, the maximum scene contrast between black and white (figure 2b). If the instrument were to scan slowly enough, allowing the detector time to respond to the input signal before it changes significantly, then the maximum scene contrast could almost be detected. However, as the scan rate increases in speed, the ability of the detector to capture the maximum scene contrast is lost and the amplitude of the output signal will be reduced (figure 2c). The output signal then represents a blur of energy that emerges from both the black and white bars. This loss in the output signal's contrast is due to the fact that the detector is integrating the contrast of the black and white bars together as it scans faster. The reason for the integrated signal from both the black and white bars is because the sampling interval of the instrument is fixed by design and the observation time over any location in the input scene is decreasing.

As mentioned in the introduction, there is a communication problem between the instrument engineers and the scientists regarding the nature of the pixel. This problem is not necessarily only attributed to language, but is also mathematical. Engineers are trained to and prefer to perform measurements and calculations in the mathematical frequency domain. Remote sensing scientists are trained to and prefer to work more in the spatial domain. Simply put, those of us working in the realm of remote sensing typically want to resolve spatial features of a landscape, a cloud field, and so on. The MTF, in units like cycles per kilometer, has the appearance of being a rather foreign quantity and can be easy to ignore. With the use of the inverse Fourier transform, the MTF can be mathematically transformed into its spatial domain representation. This representation has units of distance (e.g., kilometers) and is more intuitive to use for remote sensing scientists. The transformed MTF can be used to describe the size of each image pixel on the ground (or in other terminology the footprint) and is commonly referred to as the Point Spread Function (PSF) or sometimes as the Point Response Function (PRF). In this paper, the term PRF will be used.

How does everything that has been discussed in this section manifest itself in the imagery? This question can be answered by examining an AVHRR coastline crossing which is a clear example of a high contrast boundary (like the black and white bars) in a scene. If the signal is truly being degraded, then there should not be a sharp edge in the image across the water/land boundary. Figure 3 shows a coastline crossing which has a distinct water/land interface on the ground and which also has a water/land interface that is perpendicular (up-down) to the scan direction (left-right). It can be seen in the graph, for both the reflected energy channel (channel 2) and the thermal channel (channel 3), that there are as many as four pixels which contain

intermediate values between the plateau of land values (on the upper left) and the plateau of water values (on the lower right). The sharp coastline is not reproduced in the image data where there is one in reality and there are several pixels, instead of just one pixel, that have mixed water/land observations. The figure clearly demonstrates that as pixels gain more distance from the water/land interface, the effect of the boundary crossing diminishes slowly until the plateau is reached. To summarize the crossing in terms of distance, the actual coastline boundary which occurs over a few meters on the ground is taking over 3 kilometers to resolve in the imagery. To further restate this from a visual interpretation standpoint, a close examination of the image shows that the coastline is blurred and thus not well defined. This blurring phenomena can be explained and modeled by gaining a more detailed understanding of the PRF; the actual footprint size.

III. The PRF and the Pixel

Figure 4 shows the PRF for the AVHRR instrument whose imagery has been used in countless studies in many disciplines, including fire research. The first thing to note is that the PRF is a weighting function, for a single pixel, which describes the response of the instrument to the energy emerging from the footprint in the input scene. From figure 4 it can be seen that the actual AVHRR footprint at nadir is over 5 kilometers in diameter across. For this study, the full footprint is being defined as the input scene area from which 99% of the energy that constitutes a pixel is emerging. The nadir resolution of AVHRR is commonly calculated to be about 1.26 kilometers (Cahoon et al, 1992b; Setzer and Malingreau, 1996). At a radius of 0.63 kilometers (half of 1.26 kilometers) it can also be seen that a surface area of the size typically quoted as the instrument's resolution only accounts for 28% of the total energy of the pixel. This means that 72% of the energy that makes up one AVHRR pixel (at nadir) is from outside the scene area that is commonly assumed to be the pixel. It should also be noted that 80% of the energy of each pixel

is from a surface area that is almost 3-kilometers in diameter at nadir. Thus, the AVHRR image pixels are broadly overlapping each other.

Setzer and Malingreau (1996) present the common and largely accepted view of the overlapping pixel structure in the AVHRR imagery. This common representation can be seen to be inappropriate as a basis for interpreting the imagery in lieu of our knowledge of the PRF. To represent the information in figure 4, figure 5 shows the AVHRR PRF, derived from engineering data, superimposed on a horizontal plane which has the classical AVHRR footprint layout drawn for a sample of image pixels near the center of the image. The tremendous footprint overlap is clearly demonstrated by the PRF. One may note that the total energy for any one pixel comes from the surface area represented by over a dozen image pixels (which of course all have the same PRF). This means that the images are extremely complex representations of the original input scenes. It is only with an understanding of the PRF that we can begin to fully comprehend our analyses and the limitations of the imagery. The most common perceptions of the image pixel are not sufficient to explain the inherent underlying subtleties of the imagery. Support for our definition of the PRF can be found in the imagery.

The AVHRR PRF is used to model a sharp land/water boundary. This modeled boundary can be seen in figure 6 as the thick curve which has each individual pixel plotted as a diamond. It is similar to the coastline crossing in figure 3 in that it has four pixels that are between the plateaus of land and water pixel values. Analysis is performed on a random AVHRR image from our inventory that contains clear-sky (no clouds) coastline crossings around the African continent. The crossings are all located on a desert/water interface and are randomly selected from varying

scan line positions within the image. Like the coastline crossing in figure 3, each water/land interface is perpendicular to the scan direction. For this comparison the PRF has been converted to pixel distances and the pixel values have been normalized. Each of these randomly selected crossings are plotted as thin black lines. It can be seen that our modeled coastline crossing does represent the actual AVHRR data very well.

There are additional complexities that have been avoided in this study. The PRF can have a more complex shape in the extremities (the low energy regions) (Breaker, 1990). We have chosen to use a more refined version of the PRF than Breaker for presentation and modeling. The actual differences in values would be extremely small and would have only complicated this discussion. Additionally, the coastline modeling in figure 6 was done with a pixel centered on the water/land interface boundary. In reality, the pixel center can be offset from the interface boundary and this would skew the results slightly. Some of this skew is seen in the actual crossings in figure 6 as a 1-2 pixel (left to right) shift that exists at any normalized pixel value. It should also be noted that the examples presented have focused on AVHRR. All imagers, including SPOT and Landsat, have similarly broad PRF's relative to their typically quoted resolutions.

IV. Fire Modeling

We have developed a physical fire model which allows us to understand the fire detection limitations of the AVHRR, the DMSP-OLS, and the MODIS instruments. The modeling begins on the ground with the derived PRF for each instrument in the appropriate fire detection channel. The model is run for each instrument with the optimum case of the fire fronts passing through the center of the pixel. In much the same way in which the footprint has been examined, the behavior

of fire must be considered also. For present purposes, three different types of landscape fires are considered for evaluation in the model, with each type possessing overlapping fire characteristics. The atmosphere has been modeled using radiative transfer methods and the flame front energy has been transferred from the surface to the instrument using the appropriate solid angles for each instrument aperture. The differences in the transmission of energy within each instrument's optical system were also taken into consideration. The evaluations of fire detectability were based on selected criteria which will be defined in this section. In the end, a physically-based fire detection model has been developed in order to understand what the limitations are for fire detection using each instrument. Further, the results of the model will also provide insights into how to interpret the fire products that are being derived using various instruments and methodologies (e.g., Cahoon et al, 1992a, Elvidge et al, 1996; Flasse and Ceccato, 1996; Justice and Dowty, 1994; Kasischke et al, 1993; Lee and Tag, 1990).

Fire behaves differently across the landscape depending on a variety of parameters (e.g., fuel moisture, winds,...). But most importantly, when considering regions that are already prone to widespread fire development, the total energy release from a fire can largely be attributed to the structure of the fuels. Forest fires, with their complex fuel structure and high fuel loading, experience wide fire fronts with tremendous amounts of energy being released per unit area (figure 7a). In contrast, savannas, with a simpler fuel structure and a lower fuel loading, have more narrow flame fronts and less energy being released per unit area (figure 7b). Field programs (e.g., Alexander, 1998; Brass et al, 1996; Kaufman and Justice, 1994; Sneeuwjagt and Frandsen, 1977; Stearns et al, 1986; Stocks et al., 1996; Stocks and Hartley, 1995; Stocks and Jin, 1988) have generated data that can be used to define fire characteristics in various landscapes. The

characteristics for the three vegetation classes defined for this study are shown in table 1. For the agricultural fires category, since there is little in the way of documented field measurements, personal observations of the flame front sizes by the authors have been included and the flame front temperatures are adopted from the savanna category.

For the modeling, the flame fronts are assumed to have had the time to grow since ignition and are spreading across the landscape at an equilibrium spread rate. Fires that have either just started to spread from their ignition point or are in a smoldering state are not considered. The flame fronts are assumed to be continuous and of even depth with the depths ranging for each vegetation class as denoted in table 1. The depth of a flame front is determined using field measurements of the fire's rate of spread and nominal flame front residence time (the length of time required for the flaming zone or fire front to pass a given point (Merrill and Alexander, 1987)). The horizontal lengths of the flaming fronts are varied in order to spread across the entire range of conceivable sizes. The limits of detection, either undetectable or instrument saturation, are identified for each vegetation system as the entire ranges of depths and lengths are exploited. Only single flame fronts within a footprint have been modeled and the flame fronts are considered to be uniform. The two primary variables that control the energy release in the model are the flame front depth and length. The flame fronts can be shifted off center within a footprint, but by no more than half the distance between neighboring footprint centers (only a few hundred meters). A sensitivity study determined that the differences were not significant enough to warrant additional modeling. This analysis will concentrate only on flame fronts that pass directly through the center of the footprint.

The appropriate PRF weighting is applied to integrate the energy, both areas of flame front and background temperatures, emerging from the entire footprint area. The temperature of the flame fronts is nominally taken to be 1000 *K* and the background temperature is 305 *K*, that of a hot afternoon when fires are prevalent. The atmospheric transmission is modeled using the MODTRAN software package and the spectral response of each instrument channel that is used for fire detection has been inserted. The atmospheric modeling profiles of temperature and water vapor are those of a climatological mid-latitude summer and a very hazy environment. The atmospheric modeling for the DMSP-OLS instrument's visible wavelength channel is for nights with no moonlight and hazy skies. The threshold of detection for the thermal channels is selected based on observations of known fires found in the AVHRR imagery and knowledge of the AVHRR and MODIS fire channel noise characteristics. To gain confidence in the classification of a fire pixel, the fire pixel needs to be significantly hotter than its surrounding background temperature. For the purpose of this analysis, the difference between the pixel that contains a fire and a pixel of only the background temperature must exceed 10 *K* in order for the fire to be detected. This 10 *K* criteria has been applied to both AVHRR and MODIS in this modeling effort. In reality, the background temperature would likely be higher than the 305 *K* used in this study and would push the threshold of detection upward since a larger fire would be required to meet the detection criteria of 10 *K*. For DMSP-OLS, using a nighttime visible channel, the minimum detectable radiance has been chosen since all other pixel values will be that of the background.

The results of the modeling effort are intriguing. Figure 8 shows the relationship between fire detection for each instrument relative to the flame front area. Also, the typical range of flame

front sizes is presented for each of the three vegetation classes. Figure 8 shows that MODIS will saturate only for the largest forest fires and that AVHRR will saturate for forest fires an order of magnitude smaller in flame front area than MODIS. To saturate any instrument channel, the energy from the input scene exceeds the designed measurement range of that instrument channel and only the maximum possible value is reported. It is interesting to note that a single savanna fire front would not saturate AVHRR, but saturation by savanna fires can be found in the imagery. In this case, as seen in figure 9, multiple fire fronts can exist in close proximity and would be required to saturate the AVHRR instrument. For the minimum fire size that can be detected, MODIS ($\sim 213 \text{ m}^2$) does appear to be slightly more sensitive than AVHRR ($\sim 435 \text{ m}^2$) to small fires. However, there is a very small difference in the PRF for each instrument and even the resolution of AVHRR and MODIS are typically quoted as being the same ($\sim 1 \text{ km}$). The advantage of MODIS over AVHRR can be attributed to the MODIS platform being 128 km lower in orbit than the nominal 833 km orbit of the AVHRR platform. It is also apparent from figure 8 that the DMSP-OLS instrument can detect flame fronts an order of magnitude smaller in area ($\sim 45 \text{ m}^2$) than the smallest flame fronts that AVHRR and MODIS can detect. The ability of the DMSP-OLS instrument to detect very small fires is attributed to the unique low visible-light detection capability of that instrument (Croft, 1978).

Analyzed AVHRR imagery has been utilized to appraise the results of this modeling effort. Two AVHRR images were chosen, one covering a widespread fire event in the region of Angola, and the other covering a widespread fire event in Canada. A fire detection algorithm (Baum and Trepte, 1999) is used to classify and map the image pixels containing active fires. A cluster analysis is performed on the classified fire pixel maps that are derived from each image. The

purpose of the cluster analysis is to determine the frequency of occurrence of contiguous fire pixels (clusters) in groups of number from 0 to n , where n is the largest number of contiguous fire pixels. The results of this analysis are shown in figure 10. The forest fires cover an extensive amount of surface area and the results show that the clusters of contiguous fire pixels in the image are often large in count and that the large fire pixel clusters are very frequent in their occurrence. This means that the forest fires are not close to the limit of detection and are easy to identify. The results of the model have shown that the forest fires should be large enough to easily detect with the AVHRR instrument. For the savanna fires in Angola, the cluster analysis shows that single pixel fires are the most frequent in occurrence and the histogram does not show the lower half of the frequency distribution. This suggests that the savanna fires are much smaller in size and are on the edge of being detected by the AVHRR instrument. The model confirms this conclusion and shows that, for savanna fires, the typical fire front range stretches below the minimum detectable limit of the AVHRR instrument.

There are a few additional caveats to consider in this analysis. It is possible, particularly for AVHRR and MODIS, to claim fire detection in some instances that are below the sizes that are shown in this paper. If the fire temperature is higher than 1000 K, then more energy is being released and slightly smaller fires can be detected. If the background temperature is lower than 305 K, then less energy is needed to exceed the defined detection criteria of 10 K and smaller fires will be detected. Of course, the converse is true for cooler fire temperatures and warmer backgrounds. It is believed that the model has been run to cover the nominal cases. The 10 K criterion, chosen for the purpose of providing a statistically significant increase in temperature of a fire pixel over that of the background temperature, could be relaxed if the location of a specific

fire is known and there is confidence in the fire/no-fire judgement. It is also important to note that MODIS traded for more noise in the fire channel ($2 K$ noise equivalent difference temperature (NE Δ T)) to gain a higher saturation temperature and that AVHRR has a lower level of noise in its fire channel ($1 K$ NE Δ T). With less noise in the thermal channel being used for fire detection, the threshold of detection of $10 K$ could be relaxed slightly for the AVHRR modeling and in reality AVHRR could be slightly better or the same at detecting smaller fires as MODIS.

V. Discussion and Conclusions

For two decades it has been realized that fire detection was possible from space using meteorological satellite data. However, to date no instrument has been launched with the explicit design to monitor fires. To the knowledge of the authors, no study has evaluated the differences in fire detection limits of the instruments being used for fire monitoring. As various international projects are underway to map fires globally, having this very fundamental assessment will allow researchers to evaluate each of these developed products with a heightened awareness of their inherent limitations. More modeling is required to develop a similar understanding for each new instrument that will be used for fire detection so the derived products from each instrument can be appropriately compared. For example, MODIS does provide an advantage over AVHRR in terms of having a higher saturation temperature, but as determined in this study MODIS does not have a significant advantage over AVHRR for detecting small fires. Hence, MODIS and AVHRR active fire detection products could be compared and even appropriately combined since their results should be very similar in mapping fire activity. In addition to understanding the capabilities of the existing instruments for fire detection, this type of modeling can be used in the development of new instrumentation. One such result from this modeling effort is that a $250 m$ resolution (resolution in the conventional sense) thermal channel could provide a similar small fire detection

capability as that of the DMSP-OLS instrument. This is a worthwhile goal given that many of the agricultural fires and fires in the early stages of growth in any ecosystem will escape detection with the current systems.

The modeling approach in this analysis is physically-based and begins with the basics. The behavior of each instrument is determined and quantified in the form of the PRF. The PRF defines the actual footprint size and its weighting function. Fire behavior was considered for developing the appropriate size fire fronts and temperatures to include in the model. Fire front sizes were developed for three classes of vegetation to simulate a wide range of fire behavior characteristics that are attributed to their different fuel distributions. At each step in the process of developing the end-to-end model, the results were compared to satellite measurements. The results from the AVHRR analyses are presented in this paper, but the DMSP-OLS results are in equally good agreement with the modeling. Only after the MODIS instrument is launched can a similar comparative study be completed.

The PRF defines the radiometric footprint and provides the appropriate spatial weighting of the energy from within that footprint. The use of this weighting function prevents large fire fronts from inappropriately biasing the results. That is, if the front is further from the center of the footprint it will have less influence on the overall pixel value. This is the reality of the measurements and this reality needs to be reflected in the models. Future work in the area of the PRF will provide a more rigorous mathematical examination, but for this paper the PRF has been presented in a more qualitative manner. Part of the reason for this is to present the idea of PRF itself, and hopefully generate thought about the appropriateness of imagery interpretations and

analyses. Often, knowledge of the PRF would help to understand the results from studies like those of Belward and Lambin (1990) and Steyaert et al. (1997). Both of these studies have evaluated the ability of AVHRR to resolve spatial variations in the landscape relative to that of Landsat TM imagery and provide some insight into how large the AVHRR footprint might be. Another remote sensing research topic to think very carefully about is that of subpixel modeling. This is particularly true given how many image pixels fit within one PRF footprint (the element of a single pixel) as shown for AVHRR in figure 5. And as noted, the PRF for each instrument, regardless of the quoted resolution, is similarly broad relative to a single pixel. The PRF is a mathematical description of the actual resolution of the instruments, and to some degree the PRF can provide a mathematical basis for sharpening the imagery (Gonzalez and Wintz, 1987).

VI. References

- Alexander, M. E., B.J. Stocks, B.M. Wotton, and R.A. Lanoville, An example of multifaceted wildland fire research: The International Crown Fire Modelling Experiment, Proc. The Joint III International Conference on Forest Fire Research/14th Conference on Fire and Forest Meteorology, November 16-20, Coimbra, Portugal, 83-112, 1998.
- Baum, B. A., Q. Trepte, A grouped threshold approach for scene identification in AVHRR imagery, J. Atmos. Oceanic. Tech., 16, 793-800, 1999.
- Belward, A. S., and E. Lambin, Limitations to the identification of spatial structures from AVHRR data, Int. J. of Remote Sens., 11 (5), 921-927, 1990.
- Brass, J. A., L. S. Guild, P. J. Riggan, V. G. Ambrosia, R. N. Lockwood, J. A. Pereira, and R. G. Higgins, Characterizing Brazilian fires and estimating areas burned by using the Airborne Infrared Disaster Assessment System, Biomass Burning and Global Change, MIT Press, Cambridge, MA, Vol. 2, 561-568, 1996.
- Breaker, L. C., Estimating and removing sensor-induced correlation from Advanced Very High Resolution Radiometer satellite data, J. Geophys. Res., 95 (C6), 9701-9711, 1990
- Cahoon, Jr., D. R., B. J. Stocks, J. S. Levine, W. R. Cofer III, and K. P. O'Neill, Seasonal distribution of African savanna fires, Nature, 359 (29), 812-815, 1992a.
- Cahoon, Jr., D. R., B. J. Stocks, J. S. Levine, W. R. Cofer III, C. C. Chung, Evaluation of a technique for satellite-derived estimation of biomass burning, J. Geophys. Res., 97(D4), 3805-3814, 1992b.
- Croft, T. A., Nighttime Images of the Earth from Space, Scientific American, July, 86-98, 1978.
- Elvidge, C. D., H. W. Kroehl, E. A. Kihn, K. E. Baugh, E. R. Davis, and W. Hao, Algorithm for the retrieval of fire pixels from DMSP Operational Linescan System data, Biomass Burning and Global Change, MIT Press, Cambridge, MA, Vol. 1, 73-85, 1996.
- Fisher, P., The pixel: a snare and a delusion, Int. J. Remote Sens., 18 (3), 679-685, 1998
- Flasse, S., and P. Ceccato, A contextual Algorithm for AVHRR fire detection, Int J. of Remote Sens., Vol. 17, pp. 419-424, 1996.
- Gonzalez, R. C., and Paul Wintz, Digital Image Processing, Second Edition, Addison-Wesley Publishing Company, 1987.
- Lee, T. F., and P. M. Tag, Improved detection of hotspots using AVHRR 3.7 μm channel, Bull. Amer. Meteor. Soc., 71 (12), 1722-1730, 1990.
- Justice, C.O., and P. Dowty, IGBP-DIS Satellite Fire Detection Algorithm Workshop Technical Report, IGBP-DIS Working Paper #9, Workshop held in Greenbelt, Maryland, USA, on 25-26 February 1993, (NASA / GSFC), 1994.
- Kasischke, E. S., N. H. F. French, P. Harrell, N. L. Christensen, S. L. Ustin, and D. Barry, Monitoring of wildfires in boreal forests using large area AVHRR NDVI composite data, Remote Sens. Environ., 44, 61-71, 1993.

- Kasischke E. S., N. L. Christensen, and B. J. Stocks, Fire, global warming, and the carbon balance of boreal forests, *Ecol. Appl.*, 5 (2), 437-451, 1995.
- Kaufman, Y., and C. Justice, Fire Products, MODIS Algorithm Technical Background Document, 1994.
- Kidwell, K. B., NOAA Polar Orbiter Data (TIROS-N, NOAA-6, NOAA-7, NOAA-8, NOAA-9, NOAA-10, NOAA-11) Users Guide, National Environmental Satellite Data and Information Service, Washington, D.C., 1991.
- King, M. D., W. J. Kaufman, W. P. Menzel, and D. Tanré, Remote sensing of cloud, aerosol, and water vapor properties from the Moderate Resolution Imaging Spectrometer (MODIS). *IEEE Transactions on Geoscience and Remote Sensing*, 30, 2-27, 1992.
- Kurz, W.A., M. J. APPS, B. J. Stocks, and W. J. A. Volney, Global climate change: disturbance regimes and biospheric feedbacks of temperate and boreal forests, Biotic Feedbacks in the Global Climate System: Will the Warming Speed the Warming?, G. Woodwell (ed.), Oxford Univ. Press, Oxford, UK., 119-133, 1995.
- Matson, M., G. Stephens, and J. Robinson, Fire detection using data from the NOAA-N satellites, *Int. J. Remote Sens.*, 8 (7), 961-970, 1987.
- Merrill, D.F. and M. E. Alexander, Glossary of Fire Management Terms (Fourth Edition), National Research Council No. 26516. Ottawa, Ontario, 1987.
- Setzer, A. W., and J. P. Malingreau, AVHRR monitoring of vegetation fires in the tropics: Toward the development of a global product, Biomass Burning and Global Change, MIT Press, Cambridge, MA, Vol. 1, 25-39, 1996.
- Sneeuwjagt, R. J., and W. H. Frandsen, Behavior of experimental grass fires vs. predictions based on Rothmel's fire model, *Can. J. For. Res.*, 7, 357-367, 1977.
- Smith, W. J., Modern Optical Engineering, Mcgraw-Hill, 1966.
- Stearns, J. R., M. S. Zahniser, C. E. Kolb, and B. P. Sandford, Airborne infrared observations and analyses of a large forest fire, *Applied Optics*, 25 (15), 2554-2562, 1986.
- Steyaert, L. T., F. G. Hall, and T. R. Loveland, Land cover mapping, fire regeneration, and scaling studies in the Canadian boreal forest with 1 km AVHRR and Landsat TM data, *J. Geophys. Res.*, 102 (D24), 29581-29598, 1997.
- Stocks, B. J. and J. Z. Jin, The Great China Fire of 1987: Extremes in fire weather and fire behavior, in Proc. 1988 Annual Meeting Northwest Fire Council: Fire Management in a Climate of Change, Victoria, British Columbia, 67-79 Nov. 14-15, 1988.
- Stocks, B. J. and G. R. Hartley, Fire behavior in three jack pine fuel complexes, Canadian Forest Service, Great Lakes Stocks Forestry Centre, Sault Ste. Marie, ONT, 1995.
- Stocks, B. J., B. W. Van Wilgen, W. S. W. Trollope, D. J. McRae, F. WEIRICH, and A. L. F. Potgieter, Fuels and fire behavior dynamics on large-scale savanna fires in Kruger National Park, South Africa, *J. Geophys. Res.*, 101 (D19), 23541-23550, 1996.

Stocks, B. J., M. A. Fosberg, T. J. Lynham, L. Mearns, B. M. Wotton, Q. Yang, J-Z Jin, K. Lawrence, G. R. Hartley, J. A. Mason, and D. W. McKenny, Climate change and forest fire potential in Russian and Canadian boreal forests, *Climatic Change*, 38 (1), 1-13,. 1998

VII. Tables

Table 1: Fire Characteristics

Vegetation Class	Flame Front			
	Residence Time (s)	Speed (km/hr)	Depth (m)	Temperature Range (K)
Forest Fires (Crown Fires)	30-60	1-8	8-133	800-1100
Savannas	5-16	1-3	1-13	900-1300
Agricultural	--	--	0.2-13	900-1300

VIII. List of Figures

- Figure 1:** A simple schematic of an imaging instrument showing its three fundamental systems, the optics, the detector, and the electronics. The arrows show the direction of flow, from incoming energy on the left to the output signal on the right. After Breaker, 1990.
- Figure 2:** A three schematic drawing to demonstrate the concept of the modulation transfer function (MTF). The MTF provides a measure of how well an instrument can reproduces changes that occur in the input scene. (a) Shows an ideal scene of evenly spaced high contrast bars. (b) The ideal instrument, as it scans across the bars in 'a' will reproduce a perfect square wave showing the maximum contrast. (c) The reality is that something less than the ideal can be resolved by the instrument and the result is a loss of information from the input scene.
- Figure 3:** This is a coastline crossing along a transect (shown on the right) as seen in the AVHRR imagery. The sharp boundary of the coast is not being reproduced and it takes several pixels to complete the transition in both the reflected energy (diamonds) and the thermal energy (squares) channels.
- Figure 4:** The cross-section of the AVHRR point response function (PRF) at nadir. The 3-D view of the PRF can be seen in the upper right-hand corner. The response of the instrument at the pixel level is essentially gaussian and declines outward from the pixel center. Integrating under the surface provides the estimates of the total energy at various radii outward from the center.
- Figure 5:** The set of thick concentric rings is a top-down view of the AVHRR PRF that has been superimposed on a set of smaller overlapping rings which coincide with the classical view of AVHRR image pixels. Each ring coincides with the integrated energy levels as shown in figure 4. The number of image pixels that fall within the PRF is quite large, even at the 80% total energy level.
- Figure 6:** The AVHRR PRF has been used to model a coastline crossing (bold line) and the individual modeled pixel values are plotted (diamonds). Randomly selected coastline crossings from across the entire scan line have been plotted for comparison to the modeled results.
- Figure 7:** (a) Boreal forest fire demonstrating the intense energy released by forest fires relative to that of (b) savanna fires. Flames in the boreal fire are easily an order of magnitude higher than those of the grassland fires.
- Figure 8:** The modeled fire detection for AVHRR, MODIS, and DMSP-OLS has been drawn in as horizontal lines along the fire front area scale. The left side of each line represents the minimum detectable fire and the right side shows where each instrument will saturate. Coincidentally, the typical range of fire front sizes for three vegetation classes is also drawn.
- Figure 9:** Aircraft picture of two savanna fire fronts in close proximity to one another. The larger fire front (on the right) is being fueled by the wind and is being pushed into the wind. The left-most front is advancing in the direction from which the wind is

coming. The two fire fronts will grow into each other by which time the fuels will be burned in both directions and the fire will be suppressed.

Figure 10: The fire pixels in two AVHRR scenes are detected using a fire detection algorithm (Baum and Trepte, 1999). The clusters of contiguous pixels are identified and the number of pixels in each cluster is counted. The skew of the cluster size distributions for the forest and savanna fires are completely different. The forest fire cluster size distribution is skewed toward a large number of pixels in each cluster and the savanna fire distribution is skewed toward single pixel fires.

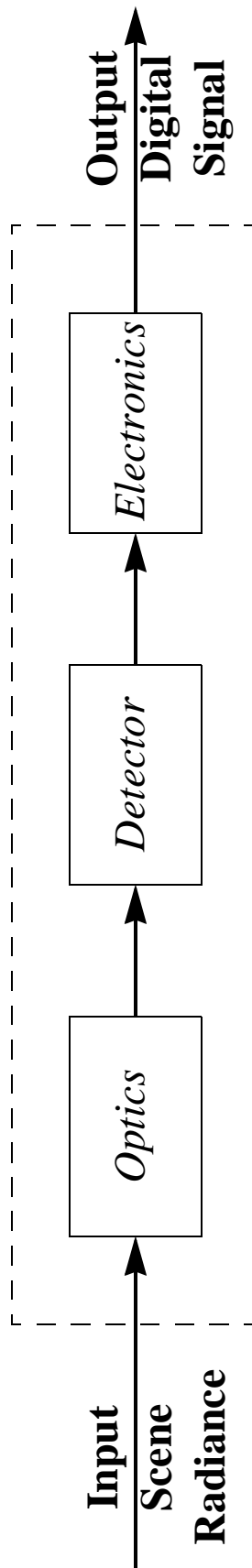


Figure 1

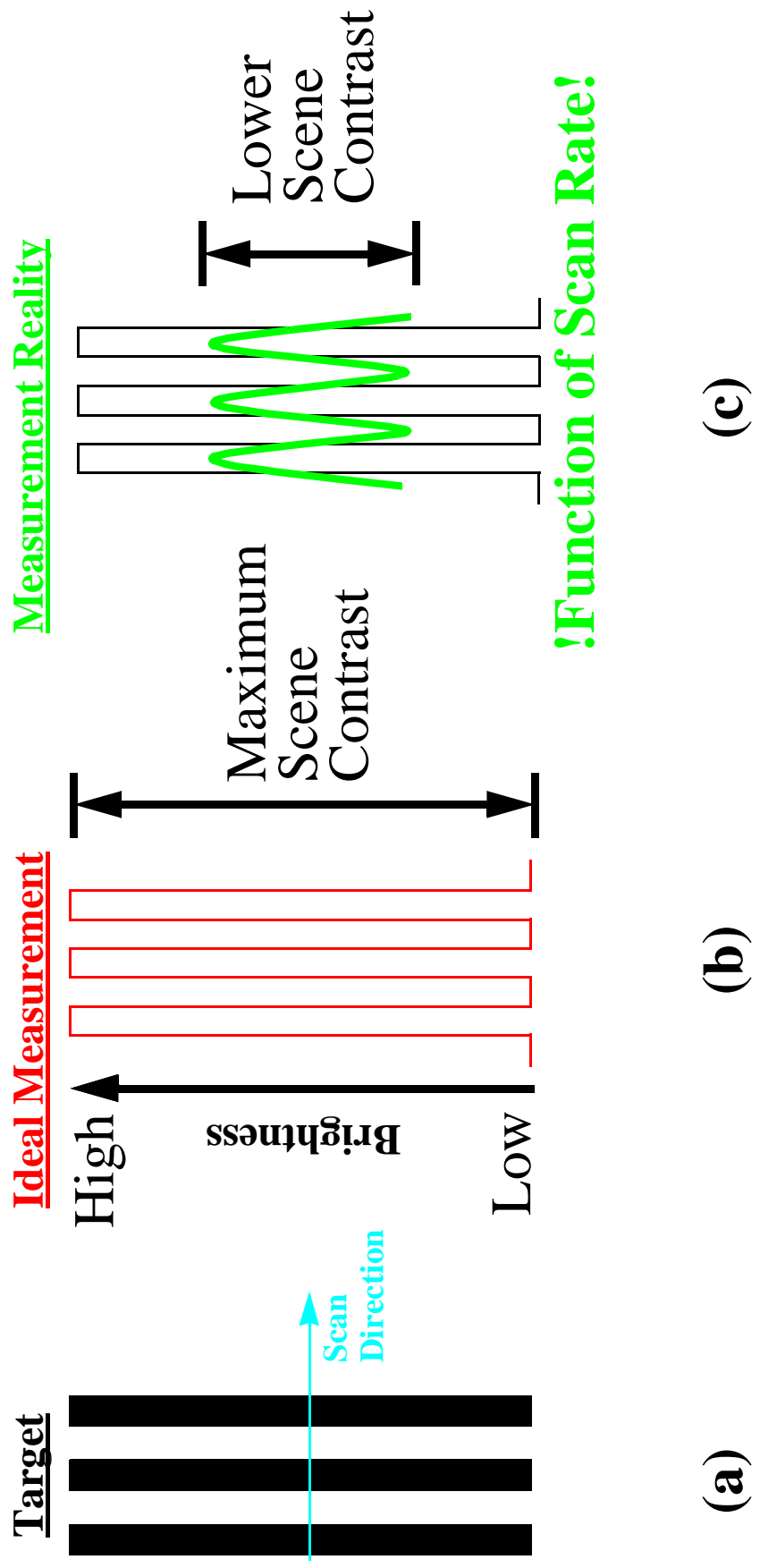


Figure 2

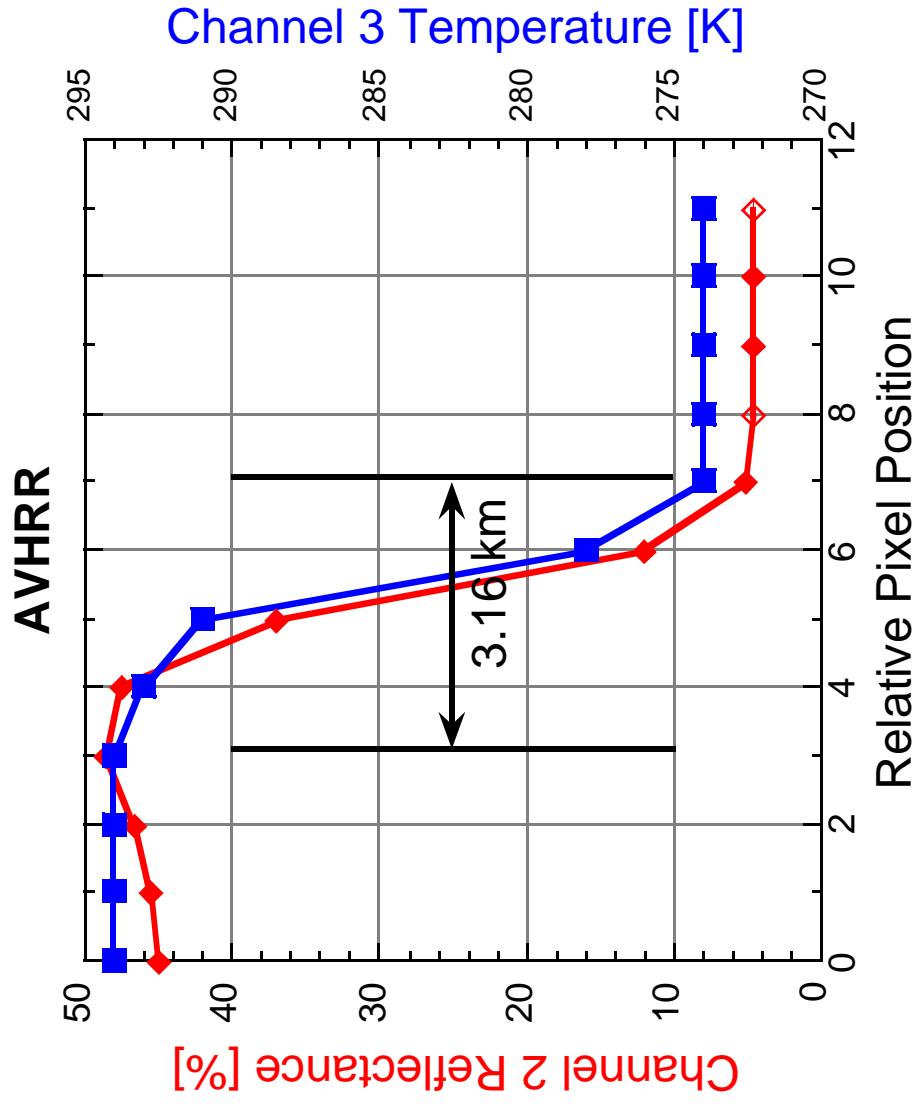
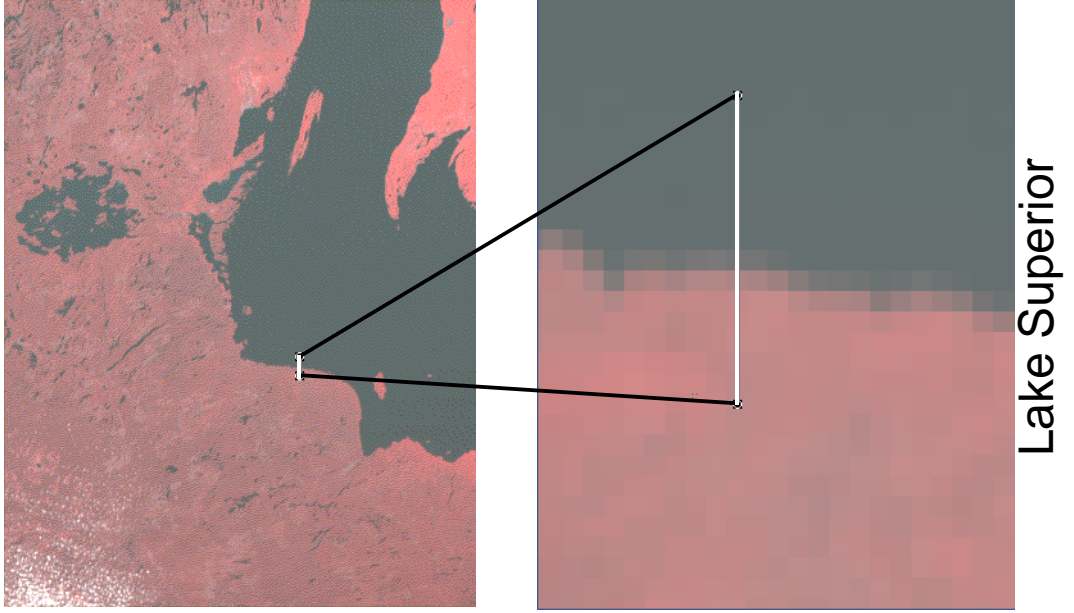


Figure 3

AVHRR Point Response Function

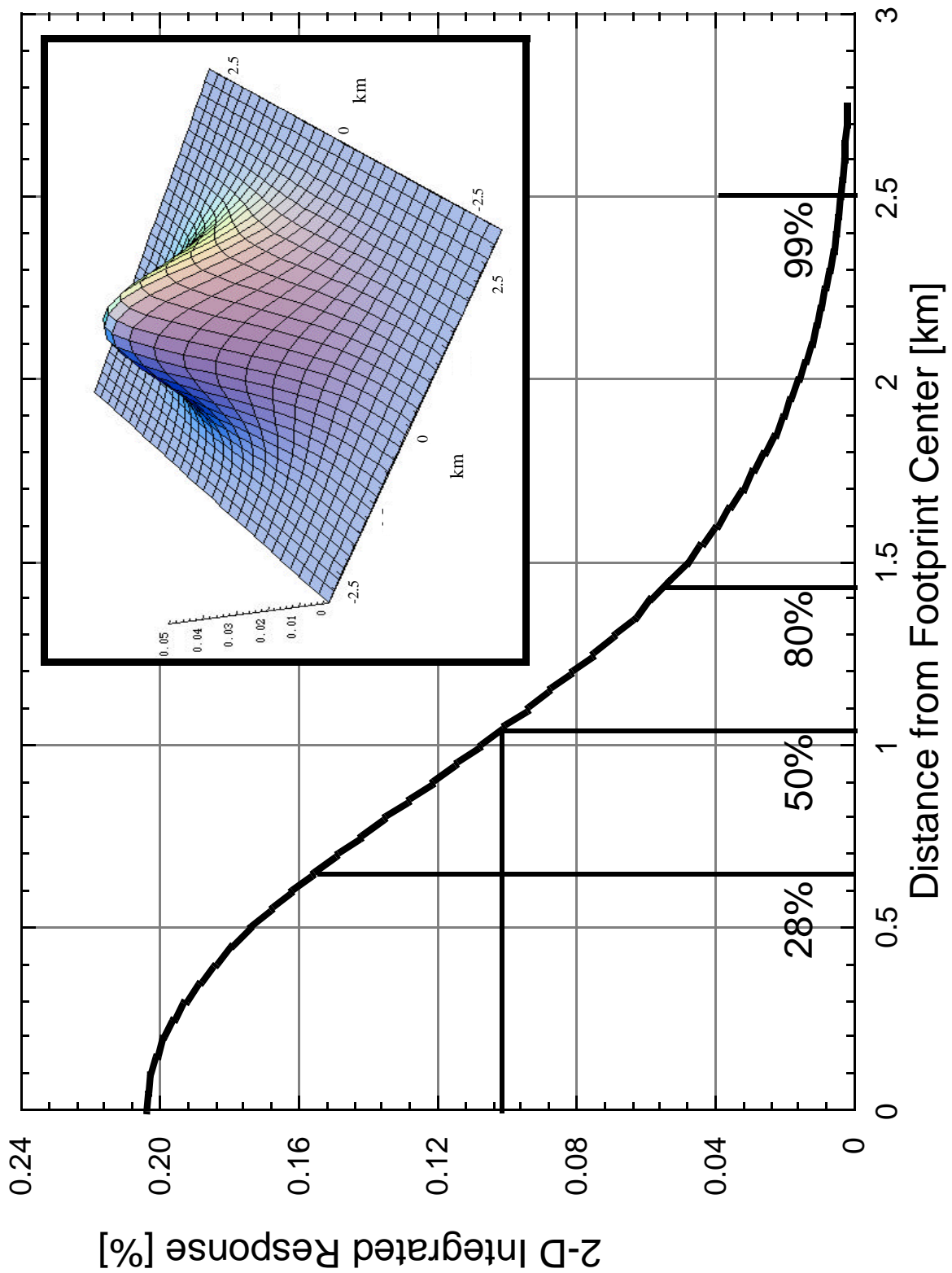


Figure 4

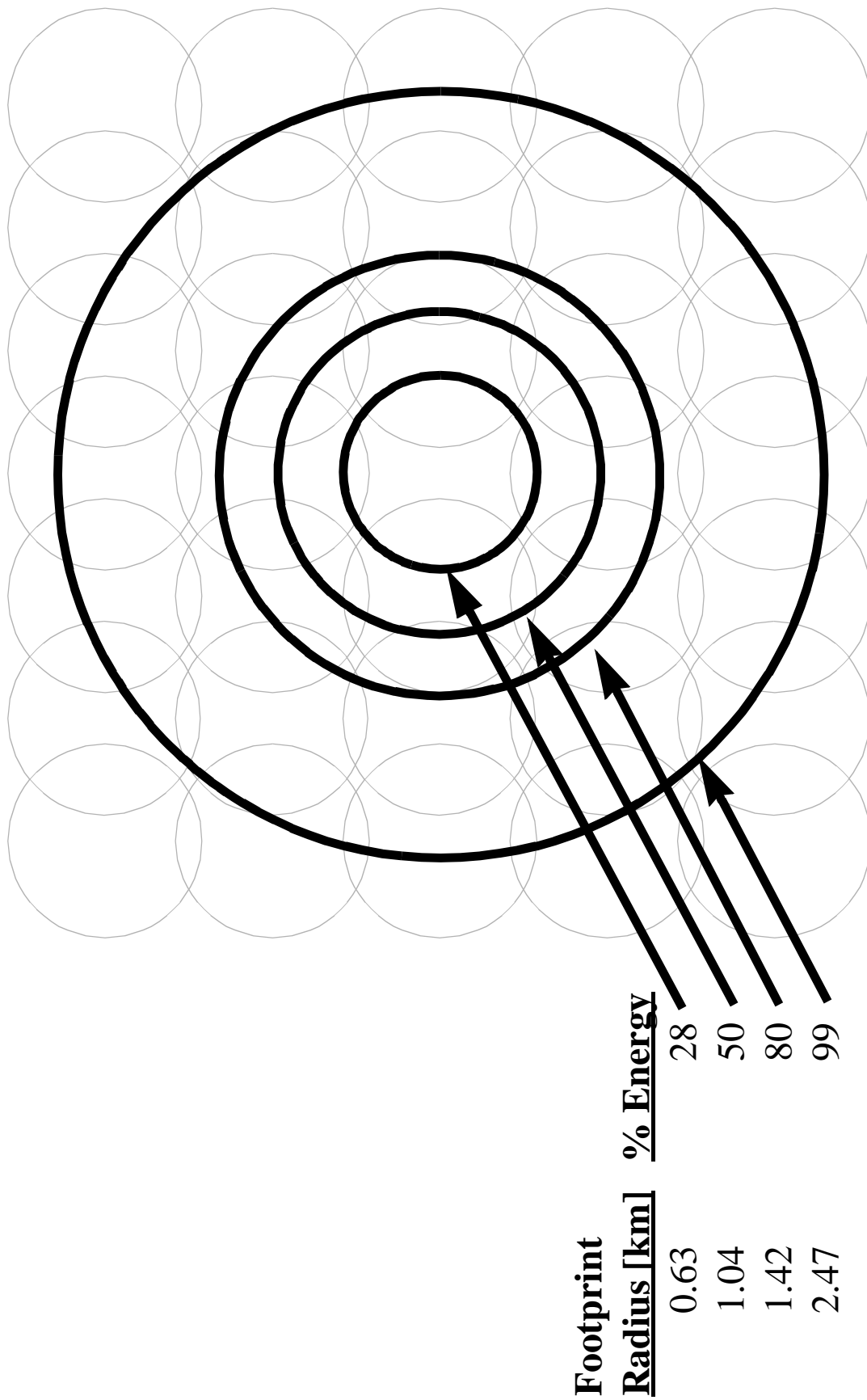


Figure 5

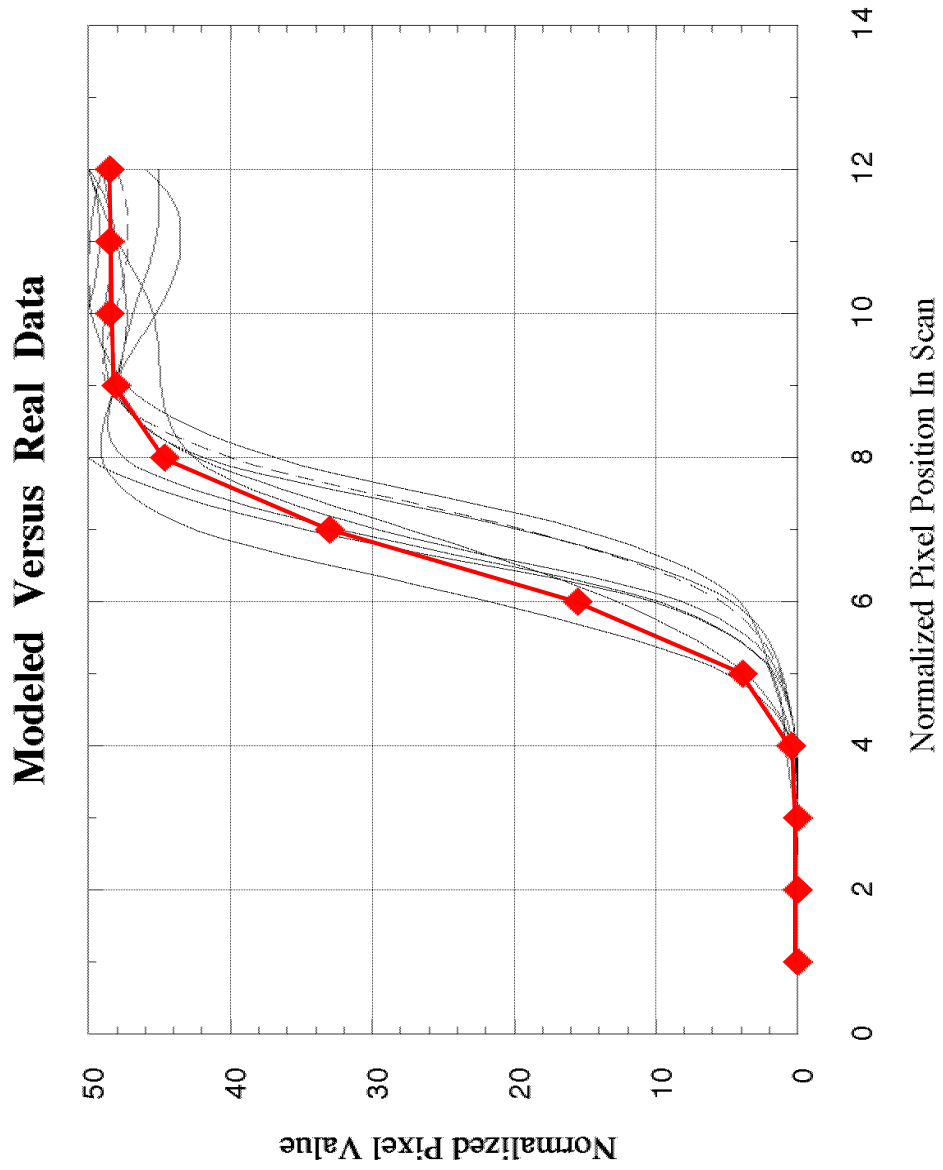


Figure 6



(a)



(b)

Figure 7

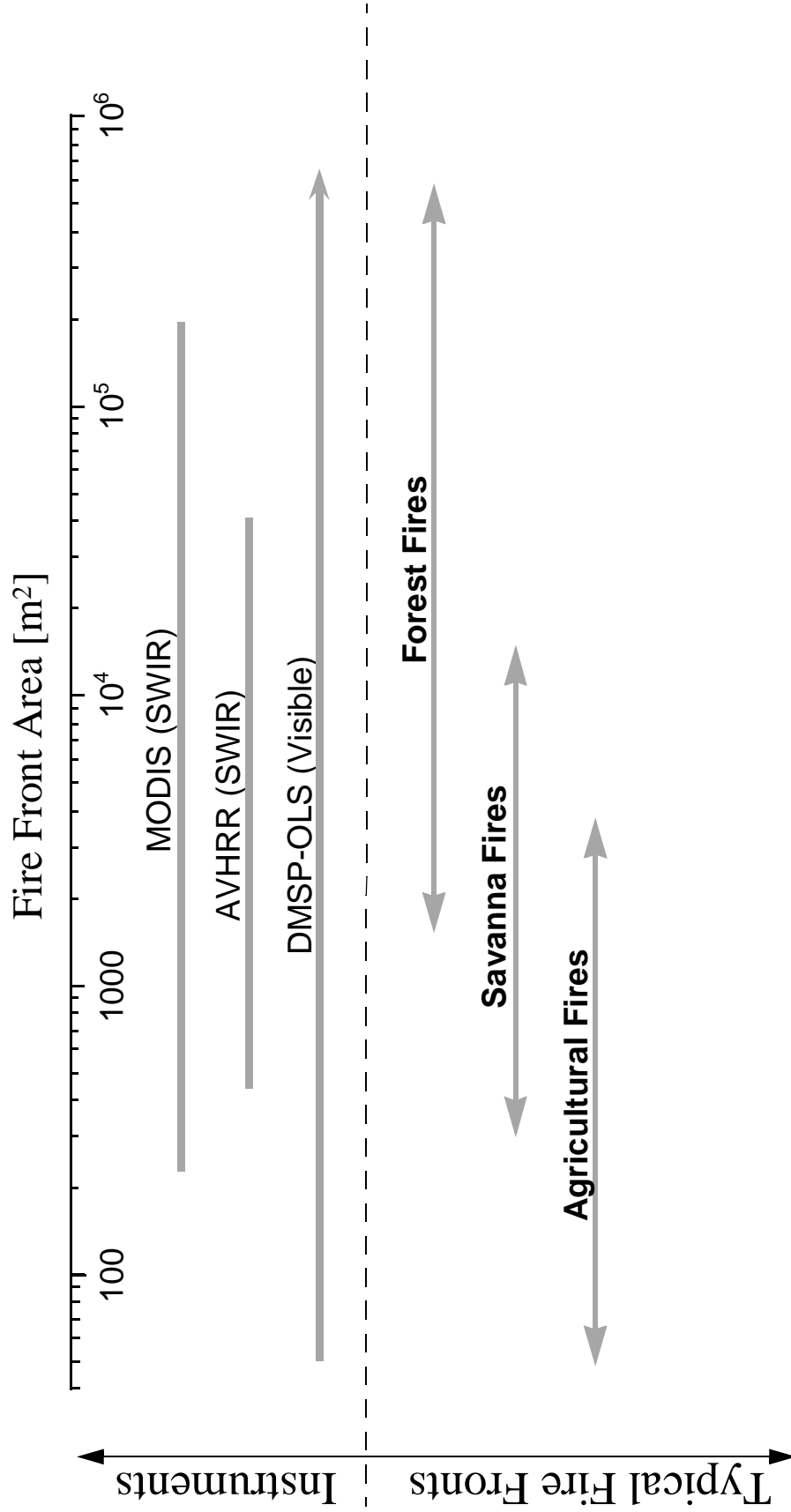


Figure 8



Figure 9

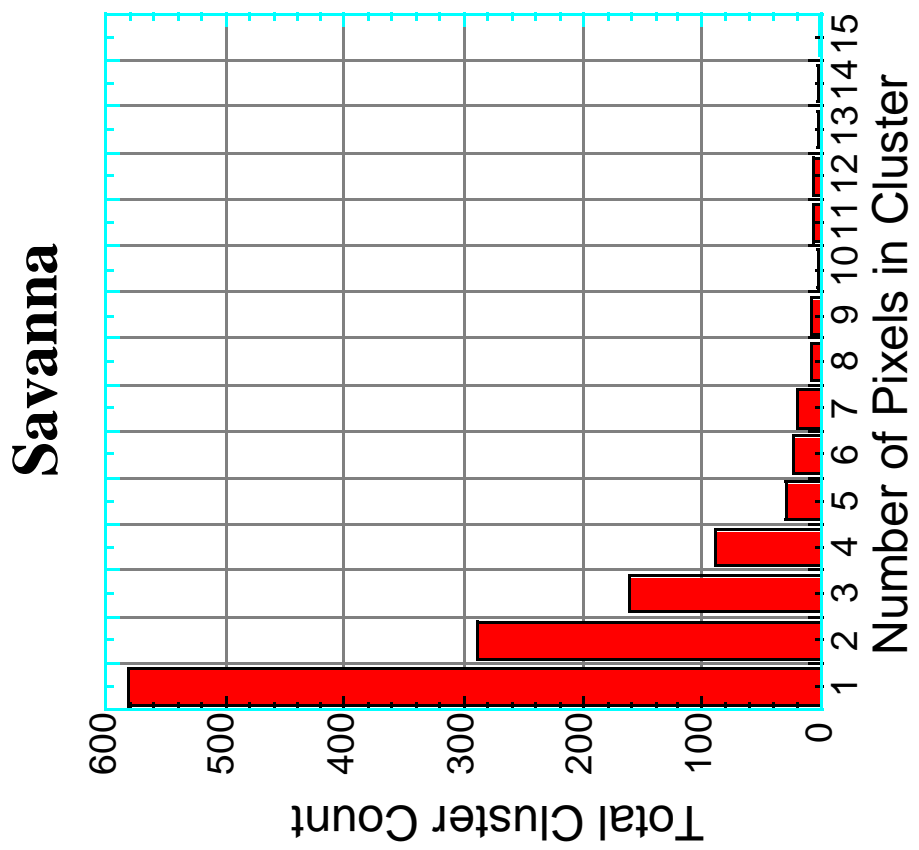
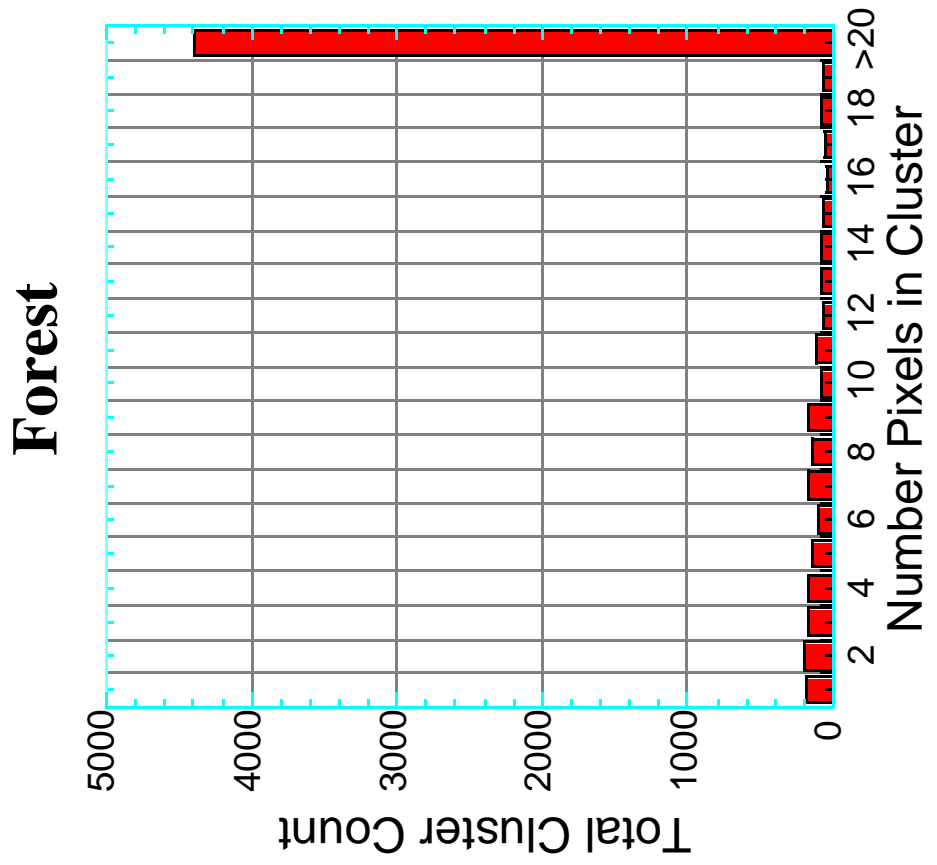


Figure 10